Analytical and Experimental Investigation of Output Feedback vs Linear Quadratic Regulator

Zoran N. Martinovic,* George C. Schamel II,* Raphael T. Haftka,† and William L. Hallauer Jr.†
Virginia Polytechnic Institute and State University, Blacksburg, Virginia

This paper presents analytical and experimental comparisons of three control laws for a laboratory structure designed to simulate large space structures. The first control law is the standard time-invariant linear quadratic regulator with state estimation, which requires model reduction for practical implementation. This model reduction may lead to spillover instability. Two simple direct output feedback controls laws guaranteeing stability are proposed. One minimizes the maximum control force, and the other minimizes the same quadratic performance index as the linear quadratic regulator. The three control laws are found to give comparable performance for the modes retained in the reduced model. However, the standard linear quadratic regulator with state estimation provides almost no margin of stability for the unmodeled modes, whereas the simpler direct feedback laws provide significant stability margins to all modes. The analytical results were verified experimentally using a digital implementation of the control laws. Good agreement between the analytical predictions and experimental measurements was observed.

Nomenclature

c = inherent damping matrix
D = active damping matrix ($n_c \times n_c$)
e = state reconstruction error vector ($2n \times 1$)
F_d = gain matrix ($n_c x 2n$) defined after Eq. (32)
FIJ = matrix partitions defined in Eq. (37)
f_c = corner frequency of low-pass filter
f_i = maximum force ratio or performance index defined in Eq. (27)
g_j = jth constraint in optimization problems
I = identity matrix of appropriate order
k = structural stiffness matrix
M_i = ith modal mass, $i = 1, \ldots, n_R$
m = mass matrix
n = number of degrees of freedom
n_c = number of control actuators
n_f = number of initial conditions
n_m = number of stability margin constraints
n_R = number of degrees of freedom of reduced model
n_s = number of sensors
q = vector of physical displacements ($n \times 1$)
q = scaling parameter in Eq. (33)
$\dot{q}_j$ = velocity measured by jth sensor, $j = 1, \ldots, n_s$
S = Riccati solution matrix for regulator design
U = applied load distribution matrix ($n \times n_c$)
u = control input vector ($n_c \times 1$)
w_1 = vector of state excitation noise ($2n \times 1$)
x = state vector of structural motion ($2n \times 1$)
y = sensor output vector
β = performance index identified in Eq. (34)
ζ = damping ratio
Φ = modal matrix ($n \times n$)
ϕ_i = open loop modal vector of mode i
ω_i = ith natural frequency
$\underline{0}$ = zero matrix of appropriate order
$\underline{\ }$ = augmented system
$\tilde{\ }$ = closed-loop system

Subscripts
E = augmented reconstructed matrix
L = lower limit
R = reduced model
0 = initial value

I. Introduction

CURRENTLY, there is great interest in the active control of large space structures. Many analytical studies are based on a linear quadratic (LQ) optimal control. However, this control strategy requires a controller that is the same order as the model of the structure. It is typically difficult to design and impossible to implement a controller that is of the same order as the finite-element model of a large space structure. Consequently, the control system is designed based on a reduced-order model of the structure including the first few vibration modes. Modal truncation of the structural model can result in a control system that destabilizes higher-order modes, a phenomenon known as spillover instability.[1] For this reason, there is interest in modifying the LQ design process to guarantee the stability of the unmodeled dynamics.[2]

Even with a reduced model of the structure, the LQ system design may be difficult to implement. For this reason many experimental studies simulating the control of large space structures have employed simple control laws.[3-6] The purpose of the present paper is to develop simpler direct output feedback control laws that guarantee system stability. One proposed law is based on the same quadratic performance index as LQ control, and the other is designed to minimize the maximum control force. The proposed control laws are compared to an LQ design for a laboratory structure designed to have some characteristics of future large space structures: low and closely spaced natural frequencies with small inherent damping.

II. Formulation of Control Techniques and Optimality Criteria

Control System Modeling

The equations of motion for a structure with n degrees of freedom (DOF) and controlled by n_c actuators are

$$m\ddot{q}(t) + c\dot{q}(t) + kq(t) = Uu(t) \tag{1}$$

Presented as Paper 87-2390 at the AIAA Guidance, Navigation, and Control Conference, Monterey, CA, Aug. 17-19, 1987; received Dec. 3, 1987; revision received Sept. 7, 1988.

*Graduate Research Assistant, Department of Aerospace Engineering. Member AIAA.
†Professor, Department of Aerospace Engineering. Member AIAA.

We assume that c does not couple the undamped modes of vibration; q is an $n \times 1$ vector of physical or generalized displacement components, and U is an $n \times n_c$ applied load distribution matrix relating the $n_c \times 1$ control point vector u to the structural DOF's. We assume these matrices are constant.

Including uncertainties and random excitation in the form of a vector $w_1(t)$, the state space equation for the system is

$$\dot{x}(t) = Ax(t) + Bu(t) + w_1(t) \tag{2}$$

with

$$A = \begin{bmatrix} -m^{-1}c & -m^{-1}k \\ I & 0 \end{bmatrix} \tag{3}$$

$$B = \begin{bmatrix} m^{-1}U \\ 0 \end{bmatrix} \tag{4}$$

and

$$x(t)^T = [\dot{q}(t)^T q(t)^T] \tag{5}$$

To prevent numerical ill-conditioning, it is desirable that the q and $\dot{q}$ components of x have the same order of magnitude. This can be achieved by using the reciprocal of a typical frequency as the time unit. In the present work, the time unit employed was 10^{-2} s (cs).

The n DOF's of the analytical model may have to be reduced to n_R to meet the physical limitations of the control hardware. The model reduction scheme used is based on the first n_R undamped modes of the system.[7] However, the reduced vector of DOF q_R is not the modal amplitudes but a subset of n_R DOF in q. The reduced matrices needed for obtaining reduced system and control matrices A_R and B_R are given as

$$m_R^{-1}c_R = \Phi_R[\text{diag}(2\zeta_i\omega_i)]_R\Phi_R^{-1} \tag{6}$$

$$m_R^{-1}k_R = \Phi_R[\text{diag}(\omega_i^2)]_R\Phi_R^{-1} \tag{7}$$

$$m_R^{-1}U_R = \Phi_R[\text{diag}(M_i^{-1})]_R\Phi_R^T U_R \tag{8}$$

The Φ_R is the $n_R \times n_R$ partition of the full modal matrix Φ containing only DOF's and modes to be retained in the reduced model. The M_i, ζ_i, and ω_i are, respectively, the modal masses, inherent damping ratios, and undamped natural frequencies of the retained modes.

Linear Quadratic Control

The standard steady-state, deterministic (i.e., $w_1 = 0$) linear quadratic regulator (LQR) has a performance index of the form

$$J = \int_0^\infty [x(t)^T Q x(t) + u(t)^T R u(t)]\, dt \tag{9}$$

where Q and R are weighting matrices.[8] The optimum value of the performance index with a given vector x_0 of initial conditions is

$$J_{\min} = x_0^T S x_0 \tag{10}$$

where S is found by solving an algebraic matrix Riccati equation. The initial conditions chosen for comparison are the first six open-loop mode shapes, each normalized with a maximum deflection of 1 in., $x_0^T = [0, \phi_i^T]$.

Since we cannot measure all of the states, and since measurement noise is present, we obtain an estimate $\hat{x}$ to the state with an observer that solves

$$\dot{\hat{x}}(t) = A\hat{x}(t) + Bu(t) + K[y(t) - C\hat{x}(t)] \tag{11}$$

where y is the sensor output vector of n_s noisy measurements, C the $n_s \times 2n$ observation matrix relating y to x, and K the observer gain matrix to be determined.[8] If a Kalman filter is used as the observer, then the filter gain matrix is found through the solution of another Riccati equation. This Riccati equation depends on the assumed system and measurement noise matrices and prescribed stability margin ("alpha shift")[9,10] of the filter poles. With this optimal estimate of the state vector, the control equation is

$$u(t) = -F\hat{x}(t) \tag{12}$$

$$F = R^{-1}B^T S \tag{13}$$

The combined system of LQR and Kalman filter is denoted linear-quadratic-Gaussian (LQG) control. For assessing the loss of performance associated with the use of an observer rather than measuring the entire state vector, we use the quadratic performance index [Eq. (9)]. The LQG control system can be described with an augmented state vector $\bar{x}$ of dimension $4n$:

$$\dot{\bar{x}}(t) = \bar{A}\bar{x}(t) \tag{14}$$

where

$$\bar{A} = \begin{bmatrix} A - BF & BF \\ 0 & A - KC \end{bmatrix} \tag{15}$$

and the augmented state vector is $\bar{x}^T = [x^T, e^T]$ where the state reconstruction error vector of order $2n$ is

$$e(t) = x(t) - \hat{x}(t) \tag{16}$$

The optimal value of the performance index [Eq. (9)] is given as

$$J_{\min} = \bar{x}_0^T \bar{P} \bar{x}_0 \tag{17}$$

where the $4n \times 4n$ matrix $\bar{P}$[8,11] is the solution of the Lyapunov equation:

$$\bar{A}^T\bar{P} + \bar{P}\bar{A} + \bar{Q} = 0 \tag{18}$$

and

$$\bar{Q} = \begin{bmatrix} Q + F^T R F & -F^T R F \\ -F^T R F & F^T R F \end{bmatrix} \tag{19}$$

We assume that the observer's initial state estimate is $\hat{x}_0 = 0$ and, therefore, the augmented initial state is $[x_0^T, x_0^T]$.

To investigate the effect of model reduction, we analyze the full-order model of the structure connected to a controller designed for the reduced model. The combined structure/controller is a linear system of order $2n + 2n_R$:

$$\dot{x}_E(t) = A_E x_E(t) \tag{20}$$

where $x_E^T = [x^T, \hat{x}_R^T]$, and

$$A_E = \begin{bmatrix} A & -BF_R \\ K_R C & A_R - K_R C_R - B_R F_R \end{bmatrix} \tag{21}$$

where a subscript R denotes the reduced form of the corresponding matrix.

The quadratic performance index for the reduced-order control sytem can be evaluated as

$$J_{\min} = x_{E0}^T P_E x_{E0} \tag{22}$$

where the matrix P_E[8,11] of order $2n + 2n_R$ is the solution of the

Lyapunov equation

$$A_E^T P_E + P_E A_E + Q_E = 0 \tag{23}$$

with

$$Q_E = \begin{bmatrix} Q & 0 \\ 0 & F_R^T R F_R \end{bmatrix} \tag{24}$$

We assume that the observer's initial state estimate is $\hat{x}_{R0} = 0$ and, therefore, the augmented initial state is $x_{E0}^T = [x_0^T, 0]$.

Minimized Maximum Force Direct Rate Feedback Control

Minimized maximum force direct rate feedback control (MFDRF) is a special case of direct output feedback control. Active vibration damping is effected by pairs of colocated velocity sensors and force actuators. The number of control pairs (n_c) is typically much smaller than the order of x, and only a vector of y of n_c velocity elements $\dot{q}_j$ of the state vector is fed back in the closed loop:

$$u(t) = -Dy(t) \tag{25}$$

or

$$u_i = -\sum_{j=1}^{n_c} d_{ij}\dot{q}_j, \qquad i = 1, \ldots, n_c \tag{26}$$

System stability is guaranteed if the active damping matrix $D(n_c \times n_c)$ is positive definite because this form of active damping can only dissipate energy.[4,12,13] We therefore require $D > 0$ as a constraint and, additionally, impose minimum stability margins on selected modes of the structure.

The performance index selected here for obtaining the gain matrix D is the minimization of the maximum actuator force, assuming that each sensor has the same velocity bound. This index is chosen because the required stability margins limit the system response, and so the objective function should minimize the size of the actuators. Assuming that each velocity bound is $\dot{q}_{\max}$, then the maximum possible actuator force $u_{\max}$ for each actuator is proportional to f_i:

$$f_i = \frac{u_{\max}}{\dot{q}_{\max}} = \sum_{j=1}^{n_c} |d_{ij}|, \qquad i = 1, \ldots, n_c \tag{27}$$

The elements of D are then determined such that the control force ratio for each actuator is less than or equal to a value γ. The variable γ is then minimized subject to constraints. The optimum design problem is formulated as

find D to minimize γ

subject to $g_j = \zeta_j - \zeta_L \geq 0, \qquad j = 1, \ldots, n_m$

and $D > 0$

and $\sum_{j=1}^{n_c} |d_{ij}| \leq \gamma, \qquad i = 1, \ldots, n_c$ (28)

where g_j are constraints on the stability of the closed-loop system expressed as lower limits ζ_L on the damping ratios ζ_j of the first n_m modes. The absolute-value function does not have continuous derivatives at zero and is replaced by a quartic polynomial near zero.[11]

For comparison with the LQG design, the performance index of Eq. (10) is calculated for the MFDRF design, for a given set of initial conditions x_0 as

$$J_{\min} = x_0^T \tilde{P} x_0 \tag{29}$$

where $\tilde{P}$ is obtained from the Lyapunov equation

$$\tilde{A}^T \tilde{P} + \tilde{P}\tilde{A} + \tilde{Q} = 0 \tag{30}$$

where

$$\tilde{A} = A - BF_D \tag{31}$$

and

$$\tilde{Q} = Q + F_D^T R F_D \tag{32}$$

The F_D is the gain matrix containing the elements of D as its only nonzero elements at the DOF's where control pairs are located.

Linear Quadratic Direct Rate Feedback Control

A second proposed direct rate feedback (DRF) control law is the linear quadratic direct rate feedback (LQDRF) control based on the quadratic performance index of the LQ design. The LQ design minimizes the quadratic performance index for all initial conditions. This is impossible to achieve with direct rate feedback. Instead, the proposed LQDRF law minimizes the quadratic performance index for initial conditions in the shape of a number n_f of natural vibration modes. That is,

$$J_{\text{LQDRF}} = \max_{x_0} \int_0^\infty [q x(t)^T Q x(t) + u(t)^T R u(t)]\, dt \tag{33a}$$

$$x_0 = [0^T \phi_i^T]^T, \qquad i = 1, \ldots, n_f \tag{33b}$$

where the scalar q is selected so that minimum stability margins are met for the n_m modes by specifying lower limits (ζ_L) on their damping ratios (ζ_i). With LQR design this is commonly achieved by scaling the Q or R matrices. Because the maximum function in Eq. (33) can have a discontinuous derivative, an equivalent formulation is used for the LQDRF design:

find q, β, and the elements of D to minimize β

such that $\int_0^\infty [q x(t)^T Q x(t) + u(t)^T R u(t)]\, dt \leq \beta$

with $x_0 = [0^T \phi_i^T]^T, \qquad i = 1, \ldots, n_f$

subject to $g_j = \zeta_j - \zeta_L \geq 0, \qquad j = 1, \ldots, n_m$

and $D > 0$ (34)

The Q and R matrices here are the same as in the LQ design. Given q and a set of initial conditions x_0, the quadratic performance index is calculated as in Eqs. (29–31) with

$$\tilde{Q} = qQ + F_D^T R F_D \tag{35}$$

The optimization problems [Eqs. (28) and (34)] were solved by using a general-purpose software package—NEWSUMT-A.[14] NEWSUMT-A is based on a penalty function approach that transforms the constrained optimization problem into a sequence of unconstrained problems. An extended interior penalty function is used together with Newton's method for solving the unconstrained problems.

III. Analytical Model and Results

Analytical Model of Control System

The control laws described in the previous sections have been applied to a small laboratory structure. The structure consists of a vertical beam and an attached horizontal crosspiece, with the vertical beam suspended by four cables in tension at its top and bottom (Fig. 1). The crosspiece was designed so that the structure would have third and fourth vibration modes with relatively close natural frequencies. The vertical beam is a uniform steel beam 80 in. long, with a rectangular cross section 2 × 1/8 in. The crosspiece is an aluminum beam 32 in. long, with a rectangular cross section

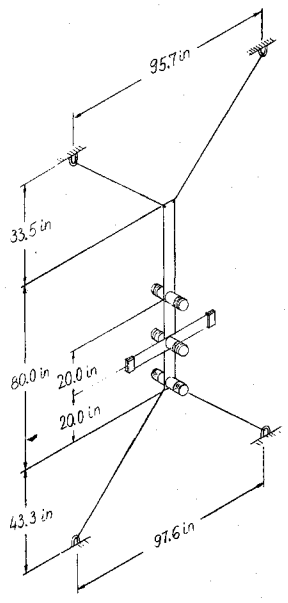

Fig. 1 Drawing of the laboratory structure.

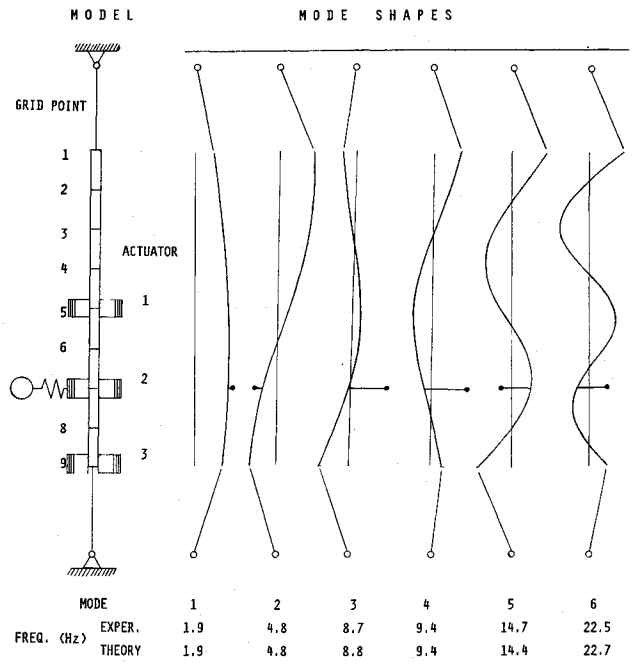

Fig. 2 Finite-element model and mode shapes.

$2 \times 1/8$ in. Small masses consisting of two ceramic magnets are located at both ends of the crosspiece, which is secured to the vertical beam by a clamp. Each stranded steel suspension cable is 0.09 in. in diameter.

Eight 10-in. beam finite elements with out-of-plane translations and bending rotations as DOF's are used to model the vertical beam. The crosspiece is symmetrical relative to the vertical beam, and only symmetrical out-of-plane motion of the crosspiece is represented in the modeling. The flexible portion of the crosspiece is modeled as a spring-mass system, as shown in Fig. 2. Therefore, the full-order model has $n = 19$ DOF's. A single string-in-tension finite element represents each cable. The model includes geometric stiffness matrices accounting for tension in the beam elements. Small lumped masses representing the control system coils, cable clamps, and the crosspiece clamp are added to the model. Inherent damping equivalent to the measured open-loop damping for only the first six modes of the structure was included in the analysis of the structure. Open-loop damping was not included for the higher-frequency modes because actual damping ratios could not be determined. (This results in analytical predictions of mild spillover instabilities in the higher-frequency modes for some control laws.) Complete details of the modeling are given in Ref. 15. Because of control hardware limitations, a reduced model of the system was also required. Only the translation DOF's at grid points 1, 3, 5, 7, 9, and the crosspiece (Fig. 2), as well as the six lowest modes (i.e., n_m) were retained.

The six lowest modes of the laboratory structure are of primary interest. Their calculated and measured natural frequencies and calculated mode shapes are shown in Fig. 2.

The structure is controlled by feedback involving three force actuators, each colocated with a velocity sensor (i.e., $n_c = n_s = 3$) as indicated by coil pairs shown in Figs. 1 and 2. Additionally, analytical results for a reduced-model LQG design were obtained with two more sensors located at grid points 1 and 3.

Analytical Results

The LQR control system was designed with $Q = I$ and $R = 0.22I$, selected to just achieve 3% damping in the first six vibration modes. For the LQDRF design the number of initial conditions n_f was six, and the optimum value of q was 0.0001, indicating that the system was designed to minimize the control effort with the response limited by the required stability margin. Additionally, the LQDRF optimization was repeated with $n_f = 3$ and 9. There were only small variations in the damping ratios and performance indices between the three cases, indicating a relative insensitivity to the number of modes used in the LQDRF design.

The MFDRF design was obtained with the same stability margins ($n_m = 6$, $\zeta_L = 0.03$). Table 1 displays the two direct rate feedback designs (i.e., matrix D) produced. The gains in the LQDRF design are seen to be substantially larger than for the MFDRF design.

The Kalman filter was designed with an alpha shift and noise matrices selected to make the real parts of the filter poles about three times larger than the real parts of the regulator poles. The alpha shift dominated the design, whereas the noise matrices had an insignificant influence. The LQG design has lower performance than an LQR design because of the use of a reduced model and state estimation. The effects of state estimation were investigated by designing a filter for the reduced-order system with five velocity sensors instead of three, introducing two noncolocated sensors, one at the top of the beam and one 20 in. down from the top. This filter was designed with the same alpha shift and system and measurement noise matrices used in the previous filter. The same feedback matrix F was used to form the closed-loop system matrix and evaluate the closed-loop roots.

Table 2 shows the damping ratios for the two DRF designs and for both the full-order LQR design and the reduced-order LQG designs [obtained from the eigenvalues of A_E, Eq. (21)]. It is seen that for the first six controlled modes the effect of the model reduction and the Kalman filter is to decrease the damping ratios by up to 20% (mode 2). The LQR damping ratios are greater than the corresponding values for the MFDRF design and, with the exception of mode 5, greater than the corresponding values for the LQDRF design, indicating that more control effort is supplied by the LQG controller than by the DRF designs. Daming ratios for the five-sensor system were nearly unchanged from the three-sensor LQG design (Table 2), indicating that most of the difference between the LQG and LQR daming ratios is probably due to model reduction.

Quadratic performance indices (using $Q = I$, $R = 0.22I$) were calculated [see Eqs. (22) and (29)] for initial conditions in the form of the first six open-loop mode shapes, and results are presented in Table 3. Since the analytical model did not include open-loop damping in the higher-frequency modes,

Table 1 Gain matrices D for DRF control (lb-s/in.)

Actuator grid point no.	5	7	9
	MFDRF control sensor grid point		
5	0.0500	0.0000	0.0000
7	0.0000	0.0359	−0.0139
9	0.0000	−0.0139	0.0222
	LQDRF control sensor grid point[a]		
5	0.0581	0.0261	−0.0011
7	0.0261	0.1018	−0.0014
9	−0.0011	−0.0014	0.0448

[a] $n_f = 6$, $Q = I$, $R = 0.22I$, $q = 0.0001$.

Table 2 Closed-loop damping ratios

Mode no.	LQR	LQG reduced-model design	LQG 5-sensor design	MFDRF	LQDRF
1	0.6221	0.5900	0.5905	0.1830	0.5589
2	0.2270	0.1881	0.1881	0.0304	0.0695
3	0.1441	0.1286	0.1293	0.0600	0.1151
4	0.0666	0.0605	0.0605	0.0301	0.0428
5	0.0567	0.0506	0.0505	0.0454	0.0613
6	0.0301	0.0278	0.0276	0.0300	0.0300

Table 3 Quadratic performance index ($Q = I$, $R = 0.22I$)

Initial conditions mode no.	LQR	LQG	LQG 5-sensor	MFDRF	LQDRF
1	43.0	57.0	56.0	97.0	63.0
2	39.0	46.0	45.0	144.0	72.0
3	27.0	32.0	32.0	45.0	32.0
4	38.0	44.0	41.0	57.0	46.0
5	62.0	73.0	94.0	65.0	68.0
6	108.0	133.0	121.0	113.0	110.0

the LQG design resulted in some low-level spillover instabilities in the higher-frequency modes, which prevented calculation of the performance indices. Therefore, small amounts of open loop damping ($\zeta = 0.001$) were added to the model, stabilizing the analytically unstable modes. This level of damping is a low estimate of the actual levels of open-loop damping present in the test structure.

Comparison of the LQR, LQG, and five-sensor LQG columns shows that the deterioration in performance due to the need for an observer is significant only for the higher modes. The effect of adding the two sensors is apparent primarily in modes 5 and 6. Mode 5 has a 29% deterioration is performance, and mode 6 has a 10% improvement. The LQG design is better than the DRF designs for the lower modes and is not as good for the higher modes. Comparison of the two direct rate feedback laws shows that LQDRF is better than MFDRF control for all but the fifth mode, which is the expected result since the LQDRF design is obtained by minimizing the LQ performance index. Comparing the LQG and LQDRF columns shows that, even though the comparison is made for the Q matrix used in the LQG design, rather than the one obtained for the LQDRF design (i.e., $qQ = 10^{-4}I$), the LQDRF performance is comparable or better, with the maximum being substantially lower. Thus, the loss of performance due to model reduction and state reconstruction for LQG control outweights the loss due to the LQDRF being suboptimal.

The effect of model reduction on the dynamics of the unmodeled modes is explored next. Table 4 compares the real parts of the regulator roots for the full and reduced-order model designs. Also given in Table 4 are the roots for both the MRDRF and LQDRF designs. Comparing the roots of the full-order and reduced-order designs, we note that the differences in the modeled modes (the first six) are not large. However, the unmodeled modes lose almost all of their stability margins, and modes 9, 10, and 18 actually became unstable (spillover instability). The differences between the three-sensor and the five-sensor LQG cases are significant for only the residual modes. Both the MRDRF and LQDRF designs, on the other hand, provided all of the modes with significant stability margins, some comparable to those of the controlled modes. This is a major advantage of the DRF designs over the LQG design, an advantage likely to be more dramatic for real-life systems for which the ratio of the numbers of modeled to unmodeled modes is much smaller.

To check on the effect of the choice of Q on the design, Q was also set to

$$Q = \begin{bmatrix} 0 & 0 \\ 0 & k \end{bmatrix} \tag{36}$$

so that $x^T Q x$ is twice the strain energy, for full state feedback. Additionally, to verify the conjecture that most of the deterioration in performance is due to model reduction, a "full-model" LQG design was analyzed where the Kalman filter was designed based on an unreduced model. The use of the energy-based Q resulted in higher damping ratios, higher performance indices, and spillover values about four times as large as the LQG design with $Q = I$.

The performance indices for the LQDRF, LQR, full-model LQG, and reduced-model LQG designs based on the Q matrix containing the stiffness matrix are compared in Table 5. All designs gave similar indices for the first mode, but significant differences started to appear in the second mode. Introducing the observer in the full-model LQG column caused less than a 5% loss of performance as compared to the LQR design. The controller designed using the reduced model but connected to the full model (LQG) has significant deterioration in performance as compared to the other three columns. This indicates that the major loss of performance in the reduced LQG design is due to the model reduction and not due to the estimator design. The LQDRF design is clearly superior to the reduced LQG design for this selection of Q, since the largest loss of performance for the LQDRF design is 9% in the fourth mode, whereas in the sixth mode the performance of the reduced LQG design is nearly eight times larger than the LQR design. The results obtained with this energy-based Q matrix reinforce the observations based on the $Q = I$ designs, and indicate that they may be insensitive to such choices.

IV. Experimental Apparatus and Procedure

Experiments were conducted to test the accuracy of the theoretical predictions against laboratory measurements of the control system performance. All of the colocated sensor-actuator control schemes (MFDRF, LQDRF, and LQG) described in the previous sections for $Q = I$ were tested on the structure using identical control hardware, but the five-sensor case and the cases designed with the energy-based Q matrix were not tested. Displacement frequency response functions (DFRF's) were measured at three positions along the beam and compared with theoretical DFRF's for the same locations.

The basic experimental apparatus and procedures are described in detail in Refs. 3, 15, and 16. A summary of the apparatus used and the procedure relevant to this paper is provided here. Figure 3 shows the overall laboratory setup, excluding the data acquisition and analysis system.

Each noncontacting velocity sensor and force actuator consisted of a small structure-borne coil moving within an annular magnetic field generated by an externally supported magnetic field assembly. Movement of a velocity sensing coil through the magnetic field produced a voltage proportional to the velocity, and application of a current to a force actuator coil produced a proportional control force.

Figure 4 is a schematic diagram of the structure and control system. Each velocity sensor voltage was first amplified by a

Table 4 Open- and closed-loop roots (1/s)

Mode	Open loop		LQG full design			LQG reduced design	LQG 5-sensor	MFDRFLQDRF	
			Regulator	Filter					
	RP[a]	IP[b]	RP	RP	IP	RP	RP	RP	RP
1	−0.05	12.0	−14.30	−40.05	11.0	−12.1	−12.1	−2.1	−6.6
2	−0.06	30.0	−7.24	−39.98	30.0	−5.9	−5.9	−0.9	−2.1
3	−0.22	55.0	−8.11	−39.89	55.0	−7.2	−7.3	−3.4	−6.4
4	−0.11	59.0	−3.97	−39.92	59.0	−3.6	−3.6	−1.8	−2.5
5	−0.26	91.0	−5.14	−39.88	91.0	−4.6	−4.6	−4.1	−5.5
6	−0.17	143.0	−4.30	−40.03	143.0	−4.0	−3.9	−4.3	−4.3
7	0.00	232.0	−2.37	−40.15	232.0	−0.47	−0.54	−0.8	−1.4
8	0.00	317.0	−3.76	−40.66	316.0	−2.1	−0.20	−2.7	−3.8
9	0.00	432.0	−2.61	−40.49	432.0	0.39	0.08	−0.8	−2.9
10	0.00	575.0	−3.58	−41.23	575.0	0.31	0.14	−2.8	−4.6
11	0.00	821.0	−1.03	−41.55	821.0	−0.031	−0.025	−0.4	−0.7
12	0.00	994.0	−2.40	−44.13	994.0	−0.030	0.005	−2.1	−3.0
13	0.00	1287.0	−1.68	−41.91	1287.0	−0.006	−0.012	−0.7	−0.9
14	0.00	1560.0	−2.78	−45.65	1560.0	−0.006	0.002	−1.8	−1.9
15	0.00	1919.0	−1.71	−42.65	1919.0	−0.008	−0.001	−0.4	−0.7
16	0.00	2403.0	−2.60	−45.42	2403.0	−0.011	0.0001	−1.3	−1.4
17	0.00	3040.0	−1.66	−41.89	3040.0	−0.00008	−0.001	−0.1	−0.5
18	0.00	3366.0	−2.95	−45.24	3366.0	0.0007	−0.0002	−0.5	−1.1
19	0.00	3622.0	−0.75	−40.35	3622.0	−0.0002	−0.00009	−0.05	−0.08

[a]RP = real part. [b]IP = imaginary part.

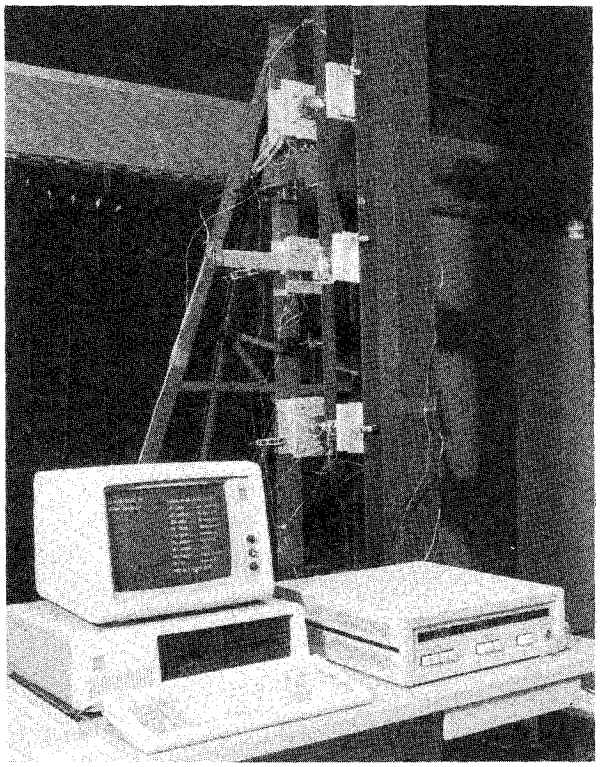

Fig. 3 Laboratory structure between sensor and actuator supports, with digital controller and host personal computer in foreground.

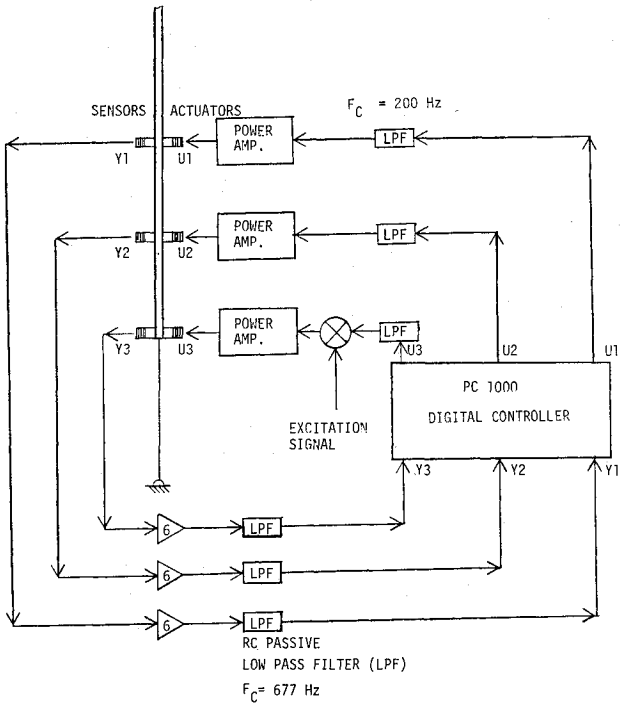

Fig. 4 Schematic diagram of the control system.

factor of six by an analog gain circuit with a very-high impedance and then filtered by a single-stage passive resistor/capacitor (RC) low-pass filter (6 dB/octave attenuation beyond f_c, the corner frequency). The low-pass filters were necessary due to radio frequency interference noise generated by the digital controller and host personal computer shown in Fig. 3. The coils and many of the instrumentation cables were not shielded, and so they apparently acted as antennas receiving the noise.

The filtered velocity signals were input to a Systolic Systems, Inc., PC-1000 digital controller, which processed the signals according to the control law being tested. The PC-1000 is a small desktop unit operated through a host IBM-PC personal computer. It has 16 channels available for input from sensors, a high-speed array processor for doing calculations with the digitized sensor singnals, and 16 channels for output signals to drive control actuators. The PC-1000 has a sampling rate variable from 2 to 2000 samples/s. When operated at high sampling rates with structural frequencies under about 20 Hz, the PC-1000 appears, for most practical purposes, to be a continuous time (analog) instrument rather than a discrete time (digital) instrument, since the phase lag produced by digital data acquisition and processing is very small. The actual time delay through the PC-1000 was found to be $1.35\Delta t$, where Δt is the sampling period.

The PC-1000's array processor performs one specific operation—multiplication of a constant 48×48 coefficient matrix

by a time-varying 48×1 vector—at the specified sampling rate. Stated mathematically, the operation is

$$\begin{bmatrix} u_{k(16\times 1)} \\ \hat{x}_{k+1(32\times 1)} \end{bmatrix} = \begin{bmatrix} F11_{(16\times 16)} & F12_{(16\times 32)} \\ F21_{(32\times 16)} & F22_{(32\times 32)} \end{bmatrix} \begin{bmatrix} y_{k(16\times 1)} \\ \hat{x}_{k(32\times 1)} \end{bmatrix} \tag{37}$$

The vector of input signals received from the sensors is y_k, u_k is the vector of output signals sent to the actuators, $\hat{x}$ the vector of "current" internal state variables, and $\hat{x}_{k+1}$ the vector of "updated" internal state variables. The $F11$, $F12$, $F21$, and $F22$ submatrices are user-specified and determine the type of control estimation filtering being applied.

The preceding matrix operation was designed to implement multivariable modern control with state estimation.[17] For MFDRF and LQDRF control law, a 3×3 submatrix of $F11$ represented the matrix D of Eq. (25), and all other elements of the 48×48 coefficient matrix were zero. These control laws were implemented at the maximum sampling rate of 2000 samples/s, closely approximating continuous-time operation.

Table 5 Quadratic performance index [using stiffness matrix in Q, Eq. (36)]

Initial conditions mode no.	LQR	LQG (full model)	LQG	LQDRF
1	34.0	35.0	35.0	36.0
2	138.0	140.0	161.0	147.0
3	158.0	162.0	266.0	168.0
4	239.0	245.0	366.0	260.0
5	577.0	602.0	950.0	593.0
6	1196.0	1227.0	10675.0	1210.0

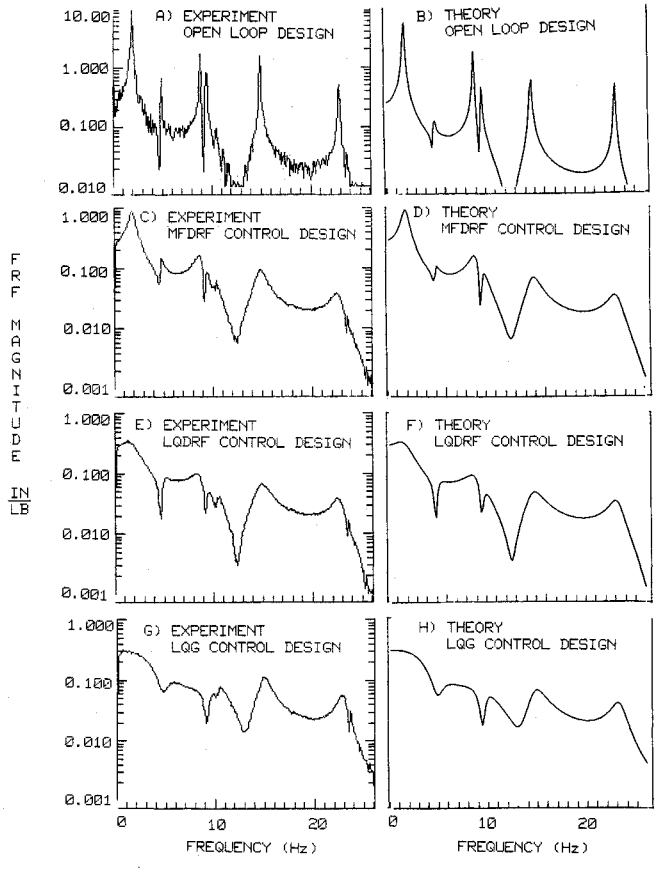

Fig. 5 Experimental and theoretical translation-to-force FRF of response at grid point 6 due to excitation at grid point 9 for: a and b) open-loop system; c and d) MFDRF design; e and f) LQDRF design; and g and h) LQG design.

LQG control requires the use of portions of the $F21$, $F12$, and $F22$ submatrices, but not the $F11$ submatrix. The LQG control law developed in the theoretical analysis section for the reduced model must be converted to a discrete-time design to be implemented by the PC-1000. This conversion process involves integration of the observer equations over one sample period, resulting in a discrete system of the form of Eq. (37). The states reconstructed by the observer $\hat{x}_{k+1}$ of reduced order $2n_R \times 1$, and the control output u_k, are determined by

$$F12 = -F_R \tag{38}$$

$$F21 = (e^{\tilde{A}_R \Delta t} - I_R)\tilde{A}_R^{-1} K_R \tag{39}$$

$$F22 = e^{\tilde{A}_R \Delta t} \tag{40}$$

where

$$\tilde{A}_R = A_R - B_R F_R - K_R C_R \tag{41}$$

The FIJ of Eqs. (38–40) occupy appropriate portions of the FIJ defined in Eq. (37).

Equations (39) and (40) were obtained by integrating the continuous-time equations across one time step, t_n to t_{n+1}. A 15-term expansion of the matrix exponential was used to evaluate Eqs. (39) and (40) at $\Delta t = 0.001$ s; Δt was chosen as small as possible subject to machine limitations so as to approximate continuous time as closely as possible. It should be noted that the discretization process does not account for the PC-1000's time delay of $1.35\Delta t$. This discretization process was checked by determining the roots of the discrete system at a sampling rate of $1/\Delta t = 1000$ samples/s in the z plane, transforming them to the s plane with the transformation[18]

$$z = e^{s\Delta t} \tag{42}$$

The poles of the discrete system matched the poles of the continuous system to three significant digits or more.

The control signals u_k generated by the PC-1000 were fitted by single-stage passive RC low-pass filters (corner frequency, 200 Hz). These filters were primarily smoothing filters present to eliminate the stair-step nature of the output signal from the PC-1000's zero-order hold digital-to-analog converter. Without these smoothing filters, a high-pitched noise radiated from the laboratory structure. Each control signal finally passed into a controlled-current power amplifier, which produced a current proportional to the input voltage to drive the actuator.

An STI-11/23 data acquisition and analysis system developed by Synergistic Technology, Inc., generated excitation signals, received measurement sensor signals, and performed all data analysis. The excitation signal was added to the control feedback signal for grid point 9, so that one actuator served the dual purpose of control actuator and exciter.

DFRF's were measured at grid points 4, 6, and 8 on the vertical beam. The displacement sensors used were noncontacting inductive-type proximity probes. Random excitation was used. To achieve a good signal-to-noise ratio, the general excitation level was set as high as possible consistent with maintaining linear behavior of the proximity probes, velocity sensors, and force actuators. Fast Fourier transforms of the response and excitation signals were calculated, and the former was divided by the latter to produce a DFRF. The frequency resolution was 0.0840 Hz. In all cases, the DFRF's calculated from a single excitation period without data windowing were reasonably smooth and repeatable, so that neither averaging nor windowing of the experimental data was necessary.

V. Comparison of Analytical and Experimental Results

Representative DFRF magnitudes for the open-loop system and the closed-loop system using the MFDRF, LQDRF, and

reduced-model LQG control laws are plotted in Figs. 5a, 5c, 5e, and 5g for experimental measurements at grid point 6 and excitation at grid point 9. The corresponding theoretical DFRF magnitudes obtained for the full-order model are plotted in Figs. 5b, 5d, 5f and 5h. The open-loop theoretical results and measurements (Figs. 5b and 5a) verify the natural frequencies of the theoretical model (i.e., 1.9 Hz, 4.8 Hz, and so on), and show realistic modeling of structural damping (which was based on experimental measurements). Good agreement of theoretical and experimental MFDRF control response is observed by comparing Figs. 5d and 5c. For example, at 1.76 Hz (first peak) the theoretical DFRF magnitude is 0.88 in./lb, and the experiment shows magnitude of 0.86 in./lb; for 4.8 Hz (second peak) the respective DFRF magnitudes are 0.11 and 0.13 in./lb; for 8.6 Hz (third peak) the DFRF magnitudes are both 0.16 in./lb, and for 19.5 Hz (antiresonance) they are 0.022 and 0.020 in./lb, respectively. The experimental results for LQDRF control also compare well with the theoretical response, Figs. 5e and 5f. The agreement for the LQG design (Figs. 5g and 5h) is as good.

The controlled system was well behaved for MFDRF and LQDRF control with no unexplained phenomena observed. This was true also for LQG control with one notable exception. The spillover instabilities predicted analytically in modes 9, 10, and 18 (Table 4) did not occur. This happened because inherent damping was not included in the analytical model of the higher-frequency modes.

VI. Concluding Remarks

An analytical and experimental investigation of three control laws for laboratory structure designed to simulate large space structures was presented. The first control law was a standard time-invariant linear quadratic regulator with state estimation, which requires model reduction for practical implementation. Two new simple direct rate feedback control laws guaranteeing stability were proposed. One minimized the maximum control force, and the other minimized the same quadratic performance index as the linear quadratic regulator. The three control laws were found to have comparable performance for the modes retained in the reduced model. However, the standard linear quadratic regulator provided almost no margin of stability against spillover instabilities for the unmodeled modes, whereas the simpler direct feedback laws provided significant stability margins to all modes. The analytical results were verified experimentally using a digital implementation of the control laws. Good agreement between the analytical prediction and experimental measurements was observed.

Acknowledgment

The research reported in this paper was supported in part by NASA Grant NAG-1-224, Contract Monitor H. M. Adelman.

References

[1]Balas, M. J., "Trends in Large Space Structures Control Theory: Fondest Hopes, Wildest Dreams," *IEEE Transactions on Automatic Control*, AC-27, No. 3, June 1982, pp. 522–535.

[2]McLaren, M. D. and Slater G. L., "Robust Multivariable Control of Large Space Structures Using Positivity," *Proceedings of the AIAA Astrodynamics Conference*, AIAA, New York, 1986, pp. 250–259.

[3]Haftka, R. T., Martinovic, Z. N., Hallauer, W. L., Jr. and Schamel, G. C., "An Analytical and Experimental Study of Control System Sensitivity to Structural Modifications," *AIAA Journal*, Vol. 25, Feb. 1987, pp. 310–315.

[4]Skidmore, G. R. and Hallauer, W. L., Jr., "Experimental-Theoretical Study of Active Damping With Dual Sensors and Actuators," *Proceedings of the AIAA Guidance, Navigation, and Control Conference*, AIAA, New York, 1985, pp. 433–442.

[5]Juang, J. N. and Horta, L. G., "Effects of Atmosphere on Slewing Control of a Flexible Structure," *Proceedings of the AIAA/ASME/ASCE/AHS 27th Structures, Structural Dynamics and Materials Conference*, Pt. 2, AIAA, New York, 1986, 613–620.

[6]Martinovic, Z. N., Haftka, R. T., Hallauer, W. L., Jr., and Schamel, G. C., II, "A Comparison of Active Vibration Control Techniques: Output Feedback Vs. Optimal Control," *Proceedings of the AIAA Dynamics Specialists Conference*, Pt. 2b, AIAA, New York, 1987, pp. 610–621.

[7]Hallauer, W. L. and Barthelemy, J. F. M., "Active Damping of Modal Vibrations by Force Apportioning," *Proceedings of the AIAA/ASME/ASCE/AHS 21st Structures, Structural Dynamics and Materials Conference*, Pt. 2, AIAA, New York, 1980 pp. 863–873.

[8]Kwakernaak, H. and Sivan, R., *Linear Optimal Control Systems*, Wiley, New York, 1972.

[9]Anderson, B. D. O. and Moore, J. B., *Linear Optimal Control*, Prentice-Hall, Englewood Cliffs, NJ, 1971, p. 50.

[10]Kammer, D. C. and Sesak, J. R., "Actuator Number Versus Parameter Sensitivity in Flexible Spacecraft Control," *Proceedings of Second Virginia Polytechnic Institute & State University/AIAA Symposium on Dynamics and Control of Large Flexible Spacecraft*, Blacksburg, VA, 1979, pp. 421–441.

[11]Martinovic, Z. N., "Sensitivity of Active Vibration Control to Structural Changes and Model Reduction," Ph.D. Dissertation, Virginia Polytechnic Inst. and State Univ., Blacksburg, VA, May 1987.

[12]Canavin, J. R., "The Control of Spacecraft Vibrations Using Multivariable Output Feedback," AIAA Paper 78-1419, Aug. 1978.

[13]Joshi, S. M., "Robustness Properties of Colocated Controllers for Flexible Spacecraft," *Journal of Guidance, Control, and Dynamics*, Vol. 9, Jan.–Feb. 1986, pp. 85–91.

[14]Thareja, R. and Haftka, R. T., "NEWSUMT-A, A General Purpose Program for Constrained Optimization Using Constraint Approximations," *ASME Journal of Mechanics, Transmission, and Automation in Design*, Vol. 107, March 1985, pp. 94–99.

[15]Schamel, G. C., II, "Active Damping of a Structure with Low Frequency and Closely Space Modes: Experiments and Theory," M.S. Thesis, Virginia Polytechnic Inst. and State Univ., Blacksburg, VA, March 1985.

[16] Haftka, R. T., Martinovic, Z. N., and Hallauer, W. L., Jr., "Enhanced Vibration Controllability by Minor Structural Modification," *AIAA Journal*, Vol. 23, Aug. 1985, pp. 1260–1266.

[17]Travassos, R. H., "The MCP-100: A Turnkey System for Implementing Multivariable Output Feedback Flight Control Laws," *Proceedings of the IEEE 1982 National Aerospace and Electronics Conference*, Inst. of Electrical and Electronics Engineers, New York, 1982, pp. 130–138.

[18]Franklin, G. F. and Powell, J. D., *Digital Control of Dynamic Systems*, Addison-Wesley, Phillipines, 1980, p. 31.